Article

Not peer-reviewed version

Sparstolonin B Suppresses Proliferation, Modulates Toll-like Receptor Signaling and Inflammatory Pathways in Human Colorectal Cancer Cells

Bürke Çırçırlı , Çağatay Yılmaz , Tuğçe Çeker , Zerrin Barut , Esma Kırımlıoğlu , Mutay Aslan *

Posted Date: 30 January 2025

doi: 10.20944/preprints202501.2224.v1

Keywords: Sparstolonin B; colorectal cancer; apoptosis; toll-like receptor; inflammation

Article

Sparstolonin B Suppresses Proliferation, Modulates Toll-like Receptor Signaling and Inflammatory Pathways in Human Colorectal Cancer Cells

Bürke Çırçırlı [1], Çağatay Yılmaz [2], Tuğçe Çeker [2], Zerrin Barut [3], Esma Kırımlıoğlu [4] and Mutay Aslan [2,*]

[1] Department of Medical Biotechnology, Institute of Health Sciences, Akdeniz University, Antalya, Turkey
[2] Department of Medical Biochemistry, Akdeniz University Faculty of Medicine, Antalya, Turkey
[3] Faculty of Dentistry, Antalya Bilim University, Antalya, Turkey
[4] Department of Histology and Embryology, Akdeniz University Faculty of Medicine, Antalya, Turkey
* Correspondence: mutayaslan@akdeniz.edu.tr

Abstract: Background: Sparstolonin B (SsnB), a natural compound with anti-inflammatory and anti-proliferative properties, was investigated for its effects on cell viability, apoptosis, and inflammatory pathways in human colorectal cancer cells (HCT-116) and healthy human fibroblasts (BJ). Phorbol 12-myristate 13-acetate (PMA), a tumor promoter and inflammatory activator, was used to stimulate proliferation and inflammatory pathways. **Methods:** HCT-116 and BJ cells were treated with SsnB (3.125–50 μM) or PMA (1–10 nM) for 12–18 hours. Cell viability was assessed using viability assays, while apoptosis was evaluated by cleaved caspase-3 staining, Terminal deoxynucleotidyl transferase dUTP nick end labeling (TUNEL), and flow cytometry. Proliferation was analyzed through proliferating cell nuclear antigen (PCNA) staining. Toll-like receptor (TLR) signaling, cytokine expression, and sphingolipid levels were measured using immunofluorescence, enzyme-linked immunosorbent assay (ELISA), and mass spectrometry, respectively. **Results:** SsnB significantly reduced HCT-116 cell viability in a dose- and time-dependent manner, with minimal effects on BJ cells. PMA stimulated proliferation, PCNA expression, and inflammatory markers, including TLR2, TLR4, MyD88, phosphorylated extracellular signal-regulated kinase (p-ERK), nuclear factor kappa-light-chain-enhancer of activated B cells (NF-kB), and cytokines TNF-α (tumor necrosis factor-alpha), IL-1β (interleukin-1 beta), IL-6 (interleukin-6). SsnB suppressed PMA-induced effects and promoted apoptosis in HCT-116 cells, increasing cleaved caspase-3, TUNEL staining, and ceramide levels while decreasing S1P (sphingosine-1-phosphate) and C1P (ceramide-1-phosphate). **Conclusions:** SsnB selectively inhibits proliferation, induces apoptosis, and modulates inflammatory and sphingolipid pathways in colorectal cancer cells, with minimal toxicity to healthy fibroblasts, supporting its potential as a targeted therapeutic agent.

Keywords: Sparstolonin B; colorectal cancer; apoptosis; toll-like receptor; inflammation

1. Introduction

Colon cancer is one of the important oncological problems in developed countries and ranks second among all cancer types in terms of incidence worldwide [1]. According to the data of the World Health Organization (WHO) in 2020, more than 1.9 million people worldwide were diagnosed with colon cancer and approximately 1 million people died due to colon cancer [1]. Colon cancer, which represents one out of every 10 cancer cases and deaths, has higher incidence and mortality rates in men than in women [1]. Combination therapy of colon cancers with polyphenols and chemotherapy has been one of the strategies used in cancer treatment in recent years [2,3]. Increasing the effectiveness of certain cancer drugs reduces the cost of treatment by shortening the length of hospital stay of patients and provides social impact. Therefore, it is considered necessary to develop

 doi:10.20944/preprints202501.2224.v1

this approach. SsnB has been classified as a polyphenol isolated from the plant roots of *Sparganium stoloniferum* [4]. Its structure is like classes of polyphenolic compounds such as isocoumarins and xanthones [5]. The structure is shown below in Scheme 1 [6] (data are computed by PubChem, https://pubchem.ncbi.nlm.nih.gov, accessed on 28 January 2025).

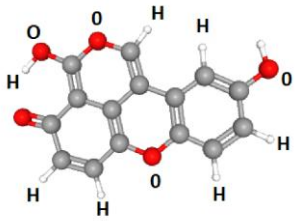

Scheme 1. Structure of Sparstolonin [6].

In this study, the efficacy of SsnB, a polyphenol that has not yet been studied as a TLR 2 and TLR 4 antagonist in colon cancer, was investigated. Toll-Like receptors recognize pathogen-associated molecular patterns (PAMPs) and regulate inflammatory responses as important components of the innate immune system [7]. However, chronic activation of TLRs leads to the formation and progression of the tumor microenvironment in many types of cancer, especially colon [8]. It has been reported that overexpression of TLR 4 promotes tumor growth and metastasis in colon cancer due to inflammation [9]. In this context, the inhibition of TLR signaling pathways is considered as a promising approach in the treatment of colon cancer. Studies have reported that TLR 2 and 4 are expressed in human HCT-116 colon cancer cell line [10–12]. The activation of TLR 2 and 4 signal transduction pathways in the human colon cancer cell line induces ERK phosphorylation, inducing cell proliferation via NF-kB and suppressing apoptosis [13]. SsnB has been shown to reduce NF-kB expression by suppressing TLR 2 and TLR 4 in gastric cancer cells and adipocytes [14–16]. Based on these findings, we hypothesized that SsnB could be antiproliferative in colon cancer cells through TLR 2 and TLR 4 signaling pathways. To the best of our knowledge, the antiproliferative effect of SsnB in colon cancer was not investigated through TLR 2 and TLR 4 signaling pathways.

The effects of sphingolipid metabolism on cancer development and progression have gained importance in recent years [17]. In a recently published study by our group, we discovered that administering 25 μM SsnB to estrogen receptor-positive breast and ovarian cancer cells dramatically reduced their S1P levels and caused a substantial buildup in intracellular concentrations of ceramides [18]. The formation of physiologically active sphingolipids is now understood to have important roles in the genesis and progression of cancer. Ceramide plays a crucial role in the metabolism of sphingolipids and suppresses tumor growth in a variety of cancerous cells by triggering apoptosis and anti-proliferative reactions [19]. According to certain studies, there may also be a connection between TLR signaling and the metabolism of sphingolipids, particularly the synthesis of ceramide, which is involved in cancer treatment [20]. Therefore, the effect of SsnB on ceramide, S1P and C1P levels were also determined in human colon cancer cells.

2. Results

2.1. Effect of Sparstolonin B on Cell Viability

The effect of SsnB (3,125-50 μM) on HCT-116 and BJ cell viability at 12, 16, and 18 hours is shown in Figure 1. Administration of 25 and 50 μM SsnB to HCT-116 cells significantly reduced cell viability at all hours relative to the control, DMSO, and other dose groups ($p<0.01$) (Figure 1A). In cells administered 6.25, 12.5 and 25 μM SsnB, 18 hours of administration within the same dose interval decreased cell viability compared to other hours ($p<0.01$). In healthy human fibroblast cells (BJ), 50 μM SsnB significantly reduced cell viability at all time intervals compared to control, DMSO, and other dose groups ($p<0.05$) (Figure 1D). After 12-hour SsnB incubation, viability in HCT-116 cells was

 doi:10.20944/preprints202501.2224.v1

calculated as 58.49 ± 9.34% (mean ± SD), indicating approximately 50% cell loss. In BJ cells, 12-hour 25 μM SsnB incubation did not significantly affect cell viability. Thus, 12-hour incubation of 25 μM SsnB was the selected dose for other experiments. PMA was used to increase proliferation in HCT-116 cells and applied to the positive control group. Its effect on cell viability was investigated in the 12-18 hours incubation interval. As shown in Figure 1B, 12-hour incubation of PMA in the range of 1-10 nM effectively stimulated proliferation in HCT-116 cells ($p<0.01$) and increased viability compared to other hours in the same dose groups ($p<0.01$). At the end of twelve-hour PMA incubation, viability in HCT-116 cells was calculated as 195.04% ± 44.94 (mean ± SD), indicating an approximately 100% cell increase. There was no effect of PMA on increasing cell viability in BJ cells (Figure 1E), and 10 nM PMA incubation at 16 and 18 hours significantly reduced cell viability compared to the other groups ($p<0.05$). As a result of the data obtained, PMA was applied at a dose of 10 nM for 12 hours in all other experiments.

In Figure 1C,F, HCT-116 and BJ cells were incubated with 1μL/mL DMSO, 25 μM SsnB, and/or 10 nM PMA for 12 h, respectively. In HCT-116 cells, incubation with PMA significantly increased cell viability compared to all other groups ($p<0.05$), while incubation with SsnB significantly decreased cell viability compared to all other groups ($p<0.05$). Cell viability was significantly reduced in the PMA + SsnB group ($p<0.05$) and it was observed that SsnB suppressed PMA activity. In healthy human fibroblast cells, the same dose groups did not produce a significant change in cell viability (Figure 1F). Light microscope images of HCT-116 and BJ cells are given in Figure 1G. While no morphological change was observed in HCT-116 cells in the control and DMSO groups, significant proliferation was observed in the PMA (10 nM, 12 hours) group. Twelve-hour administration of 25 μM SsnB altered the morphology of HCT-116 cells, resulting in clustering, shrinkage, and toxicity. No significant morphological changes were observed in BJ cells.

Figure 1H shows PCNA immunofluorescence staining in HCT-116 and BJ cells, while Figure 1I, 1K reports the amount of PCNA fluorescence staining, respectively. PCNA immunofluorescence staining and quantitation gave similar results in BJ cells in all experimental groups. In HCT-116 cells, after 12 hours of incubation, PMA (10 nM) application brought PCNA fluorescence staining to 213.34% ± 38.04 (mean ± SD) and showed an increase of approximately 100% compared to the control. After twelve hours of incubation, SsnB (25 μM) application reduced PCNA fluorescence staining in HCT-116 cells to 37.51 ± 5.89 (mean ± SD), indicating a reduction of approximately 40% compared to the control. The amount of PCNA fluorescence in the SsnB group did not show a significant change compared to the PMA+ SsnB group. PCNA quantitation data obtained in HCT-116 cells are consistent with cell viability results. The amount of PCNA protein was also measured by ELISA method in HCT-116 and BJ cells, and the results are reported in Figures 1J and 1L, respectively. The measured PCNA protein levels generally corresponded with the amount of fluorescent staining. However, the amount of PCNA fluorescence staining did not differ significantly between SsnB and PMA + SsnB groups in HCT-116 cells, while protein levels increased significantly in the PMA + SsnB group compared to the SsnB group ($p<0.01$).

 doi:10.20944/preprints202501.2224.v1

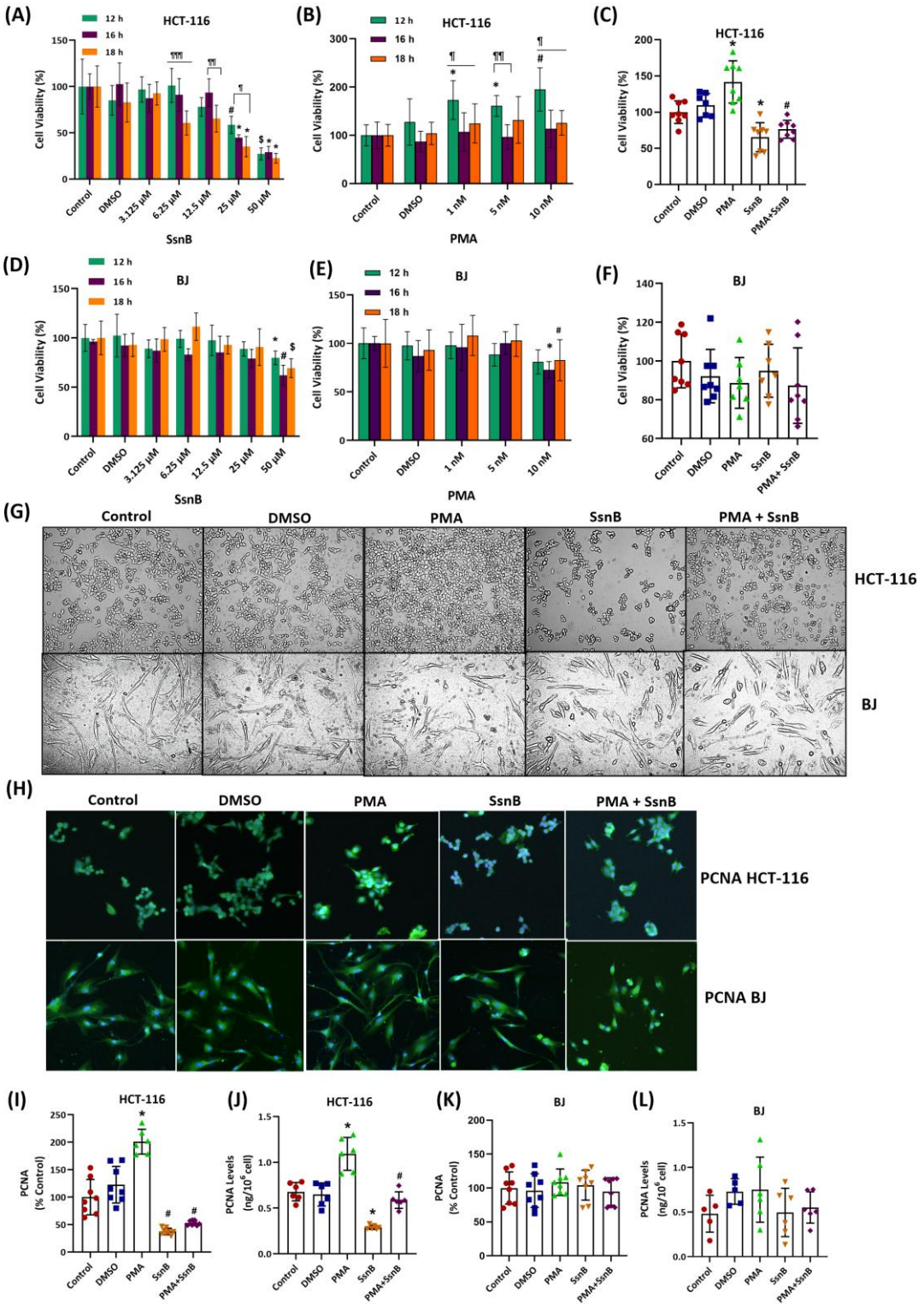

Figure 1. Cell viability and proliferation in HCT-116 and BJ cells. **(A)** Values are mean ± SD and n=8. Statistical analysis was by 2-way ANOVA with Tukey's multiple comparisons. #, p<0.01 vs. control, DMSO, 3.125 and 6.25 µM groups within the same incubation period. *, p<0.001 vs. control, DMSO, 3.125, 6.25 and 12.5 µM groups within the same incubation period. $, p<0.001 vs. all other groups within the same incubation period. ¶¶¶, p<0.01 18 h vs. 12 h and 16 h. ¶¶, p<0.01 18 h vs.16 h. ¶, p<0.01 18 h vs.12 h. **(B)** Values are mean ± SD and n=8. Statistical analysis was by 2-way ANOVA with Tukey's multiple comparisons. *, p<0.05 vs. control within the same incubation period. #, p<0.01 vs. control and DMSO within the same incubation period. ¶, p<0.01 12 h vs.16 h and 18 h. ¶¶, p<0.01 12 h vs.16 h. **(C)** HCT-116 cells were treated with DMSO (1 µL/mL), SsnB (25 µM), and/or PMA (10 nM) for 12 h. Values are mean ± SD and n=8. Statistical analysis was by one-way ANOVA with Tukey's

 doi:10.20944/preprints202501.2224.v1

multiple comparisons. *, p<0.05 vs. all other groups. #, p<0.05 vs. DMSO and PMA. **(D)** Values are mean ± SD and n=8. Statistical analysis was by 2-way ANOVA with Tukey's multiple comparisons. *p< 0.05 vs. control DMSO and 6.25 μM groups within the same incubation period. #, p<0.05 vs. control, DMSO, 3.125, 6.25 and 12.5 μM groups within the same incubation period. $, p<0.05 vs. all other groups within the same incubation period**. (E)** Values are mean ± SD and n=8. Statistical analysis was by 2-way ANOVA with Tukey's multiple comparisons. *, p< 0.05 vs. control, 1 and 5 nM groups within the same incubation period. #, p<0.05 vs. 1 nM group within the same incubation period. **(F)** BJ cells were treated with DMSO (1 μL/mL), SsnB (25 μM), and/or PMA (10 nM) for 12 h. Values are mean ± SD and n=8. **(G)** HCT-116 and BJ cells were treated with DMSO (1 μL/mL), SsnB (25 μM), and/or PMA (10 nM) for 12 h. Images were acquired via a 40× objective. **(H)** Proliferating cell nuclear antigen (PCNA) was immunofluorescent stained in HCT-116 and BJ cells treated with DMSO (1μ/ml), SsnB (25 μM), and/or PMA (10 nM) for 12 hours (40× objective). **(I)** PCNA fluorescence staining in HCT-116 cells was quantified using ImageJ software. Values are mean ± SD and n=8. Statistical analysis was by one way ANOVA with Tukey's multiple comparisons. *, p < 0.001, vs. all other groups. #, p < 0.01, vs. control, DMSO and PMA groups. **(J)** Levels of PCNA protein in HCT-116 cells. Values are mean ± SD and n=6. Statistical analysis was by one way ANOVA with Tukey's multiple comparisons. *, p < 0.01, vs. all other groups. #, p < 0.01, vs. SsnB. **(K)** PCNA fluorescence staining in BJ cells is quantified using ImageJ software. Values are mean ± SD and n=8. **(L)** Levels of PCNA protein in BJ cells. Values are mean ± SD and n=6.

2.2. Effect of Sparstolonin B on TLR2-TLR4 Signaling Pathway

Figures 2A and 2B show the amount of TLR2 and TLR4 mRNA, respectively. Figures 2C and 2D report the amount of TLR2 and TLR4 protein, respectively. TLR2 mRNA levels showed a statistically significant increase (p<0.05) in cells treated with PMA (10 nM) and PMA (10 nM) + SsnB (25 μM) for 12 hours compared to the group of cells treated with SsnB (25 μM) alone (Figure 2A). In accordance with the mRNA amounts, TLR2 protein levels were also significantly increased in the groups treated with PMA and PMA + SsnB compared to other groups (p<0.001) (Figure 2C). TLR4 mRNA levels showed a statistical increase in the PMA-treated cell group compared to the SsnB group (p<0.01) (Figure 2B). In accordance with mRNA levels, the amount of TLR4 protein was significantly higher in cells that received PMA compared to all other groups (p<0.001) (Figure 2D).

 doi:10.20944/preprints202501.2224.v1

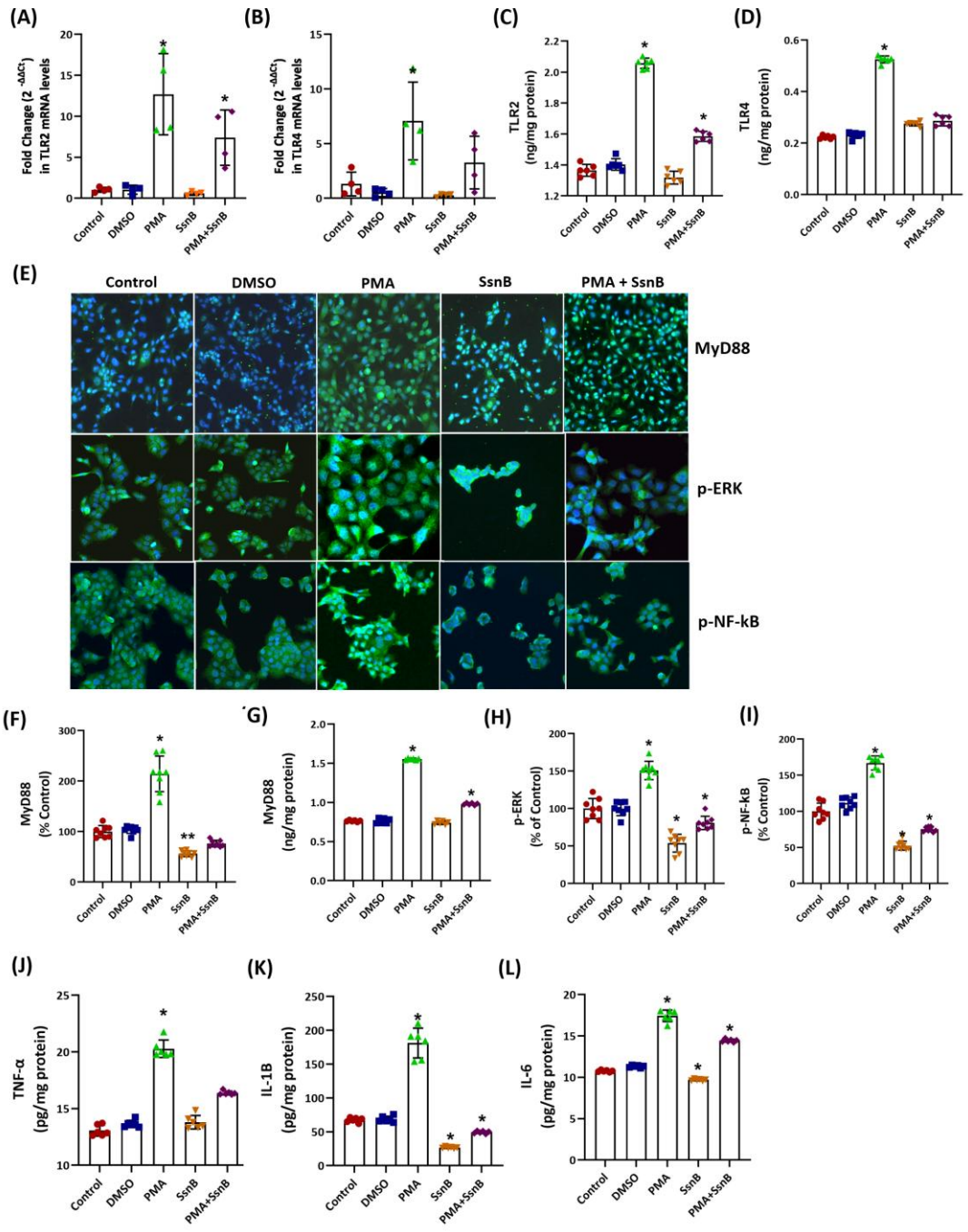

Figure 2. Evaluation of the TLR2-TLR4 signaling pathway in HCT-116 cells. Cells were treated with DMSO (1 µL/mL), SsnB (25 µM), and/or PMA (10 nM) for 12 h in all experiments. **(A)** PCR analysis of TLR2. Data shows mean ± SD and n=4 different measurements. Statistical analysis was performed by Kruskal-Wallis test and the difference between the groups was determined by Tukey's test. *, $p<0.05$ vs. SsnB. **(B)** PCR analysis of TLR4. Data shows mean ± SD and n=4 different measurements. Statistical analysis was performed by Kruskal-Wallis test and the difference between the groups was determined by Tukey's test. *, $p<0.01$ vs. SsnB. **(C)** Protein levels of Toll-like Receptor 2 (TLR2). Data shows mean ± SD and n=6 different measurements. Statistical analysis was by one way ANOVA with Tukey's multiple comparisons. *, $p<0.001$ vs. all other groups. **(D)** Protein levels of TLR4. Data shows mean ± SD and n=6 different measurements. Statistical analysis was by one way ANOVA with Tukey's multiple comparisons. *, $p<0.001$ vs. all other groups. **(E)** Myeloid differentiation primary response protein (MyD88), phospho-ERK and phospho-NF-kB was immunofluorescent stained in HCT-116 cells. (40× objective). **(F)** MyD88 fluorescence staining was quantified using ImageJ software. Values are mean ± SD and n=8. Statistical analysis was by one way ANOVA with Tukey's multiple comparisons. *, $p < 0.001$, vs. all other groups. **, $p < 0.001$, vs. control and DMSO groups. **(G)** Protein levels of MyD88. Data shows mean ± SD and n=6

 doi:10.20944/preprints202501.2224.v1

different measurements. Statistical analysis was by one way ANOVA with Tukey's multiple comparisons. *, p<0.001 vs. all other groups. **(H)** Phospho-ERK fluorescence staining was quantified using ImageJ software. Values are mean ± SD and n=8. Statistical analysis was by one way ANOVA with Tukey's multiple comparisons. *, p < 0.01, vs. all other groups. **(I)** Phospho-NF-kB fluorescence staining was quantified using ImageJ software. Statistical analysis was by one way ANOVA with Tukey's multiple comparisons. *, p<0.001 vs. all other groups. **(J)** Protein levels of tumor necrosis factor alpha (TNF-α). Data shows mean ± SD and n=6 different measurements. Statistical analysis was by Kruskal-Wallis test and the difference between the groups was determined by Dunn's multiple comparisons. *, p<0.05 vs. control, DMSO and SsnB. **(K)** Protein levels of interleukin 1B (IL-1B). Data shows mean ± SD and n=6 different measurements. Statistical analysis was by one way ANOVA with Tukey's multiple comparisons. *, p<0.05 vs. all other groups. **(L)** Protein levels of IL-6. Data shows mean ± SD and n=6 different measurements. Statistical analysis was by one way ANOVA with Tukey's multiple comparisons. *, p<0.001 vs. all other groups.

Figure 2E shows MyD88, p-ERK, and p-NF-kB immunofluorescence staining. Figures 2F and 2G report the quantitation of MyD88 fluorescence staining and ELISA protein measurement results, respectively. MyD88 fluorescence staining and protein levels were significantly increased in PMA-treated cells compared to all other groups (p<0.001). While MyD88 fluorescence staining was significantly reduced in cells incubated with SsnB compared to the control and DMSO groups (p<0.001), no statistically significant decrease in the amount of protein was detected. Similarly, while the amount of MyD88 fluorescence staining in the PMA + SsnB group did not show a statistically significant difference compared to the control and DMSO groups, ELISA protein measurement results indicated a statistically significant increase compared to the other groups (p<0.001).

Figure 2H, 2I report the quantitation results of fluorescence staining p-ERK and p-NF-kB, respectively. While p-ERK and p-NF-kB fluorescence staining increased significantly in PMA cells compared to all other groups (p<0.01), p-ERK and p-NF-kB fluorescence staining decreased significantly in cells incubated with SsnB compared to all other groups (p<0.001).

Figures 2J, 2K, and 2L show the protein levels of TNF-α, IL-1B, and IL-6, respectively. TNF-α cytokine levels were significantly increased in the PMA group compared to the control, DMSO and SsnB groups (p<0.05) (Figure 2J). IL-1B and IL-6 levels increased significantly in the PMA groups compared to all other groups (p<0.05) and decreased significantly in the SsnB groups (p<0.001).

2.3. Effect of Sparstolonin B on Apoptosis

Figure 3A shows cleaved caspase-3 and TUNEL fluorescent staining. Figures 3B and 3C report the quantity of cleaved caspase-3 and TUNEL fluorescent staining, respectively. The amount of cleaved caspase-3 fluorescence staining was significantly increased in the SsnB treated groups compared to the control, DMSO and PMA groups (p<0.01). TUNEL staining was significantly increased in the SsnB treated group compared to all other groups (p<0.01). PMA application reduced TUNEL fluorescence staining and the number of TUNEL-stained cells increased significantly in the PMA + SsnB group compared to the control group only (p<0.05).

Figure 3D shows flow cytometry graphs of Annexin-FITC and PI-labeled cells. Figure 3E reports the quantitative analysis of Annexin and PI labeled cells. The number of viable cells decreased statistically in the SsnB group compared to all other groups (p<0.05). The number of early apoptotic cells statistically increased in the SsnB group compared to all other groups (p<0.05). The number of late apoptotic cells increased significantly in the SsnB group compared to the control and PMA groups (p<0.05).

 doi:10.20944/preprints202501.2224.v1

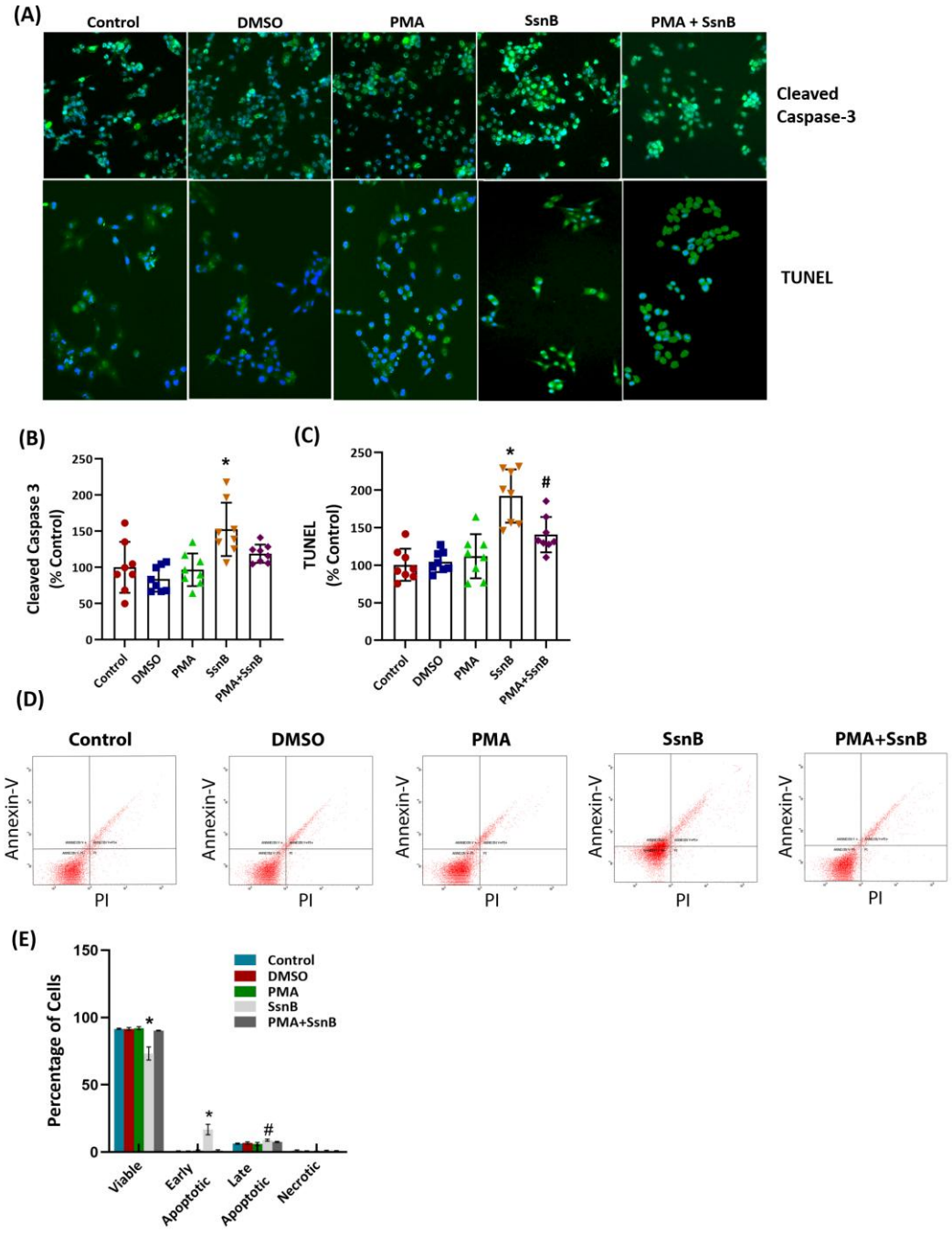

Figure 3. Apoptosis in HCT-116 cells. Cells were treated with DMSO (1 μL/mL), SsnB (25 μM), and/or PMA (10 nM) for 12 h in all experiments. **(A)** Representative immunofluorescent cleaved caspase-3 and TUNEL staining. Double-labeled images were obtained using a 40x objective lens. **(B)** Cleaved caspase-3 fluorescence staining was quantified using ImageJ software. Values are mean ± SD and n=8 different measurements. Statistical analysis was by one way ANOVA with Tukey's multiple comparisons. *, $p < 0.01$, vs. control, DMSO and PMA. **(C)** TUNEL staining was quantified using ImageJ software. Values are mean ± SD and n=8. Statistical analysis was by one way ANOVA with Tukey's multiple comparisons. *, $p < 0.01$, vs. all other groups. #, $p<0.05$ vs. control. **(D)** Representative analysis of apoptosis in HCT-116 cells by Annexin V–FITC and PI labeled flow cytometry. In each panel, the lower left quadrant shows viable cells, the upper left quadrant shows early apoptotic cells, the upper right quadrant shows late apoptotic cells, and the lower right quadrant shows necrotic cells. 10,000 cells were gated and analyzed for each condition. (**E)** Quantitative analysis of Annexin-V and PI labeling in HCT-116 cells experimental groups by flow cytometry. Data are representative of three separate experiments and values are given as mean ± SD. Statistical analysis was performed by one-way ANOVA analysis. The difference between

 doi:10.20944/preprints202501.2224.v1

groups was determined by the Tukey test. *, p<0.05, compared to control, DMSO, PMA and PMA+SsnB groups. #, p<0.05, compared to control and PMA groups.

2.4. The Effect of Sparstolonin B on Sphingolipid Levels

Table 1 reports the levels of sphingolipids measured in groups of cells. A statistically significant increase in C18, C20, C22, and C24 ceramide levels was detected in cells treated with SsnB compared to all other groups (p<0.01). A significant increase in the amount of S1P and C1P was observed in the cell groups treated with PMA compared to the other groups (p<0.01). S1P levels showed a statistical decrease in the PMA + SsnB group compared to the PMA group (p<0.01), but the measured levels were significantly higher than in the control, DMSO, and SsnB groups (p<0.01). Similarly, C1P levels showed a statistical decrease in the PMA + SsnB group compared with the PMA group (p<0.01), but the measured levels were significantly higher than the DMSO and SsnB groups (p<0.05).

Table 1. Sphingolipid levels in HCT-116 cells.

	Control	DMSO	PMA	SsnB	PMA + SsnB
Sphingolipids					
16:0 SM (d18:1/16:0)	357.84 ± 188.76	389.33 ± 101.59	288.43 ± 98.55	399.96 ± 195.80	179.05 ± 25.01
18:0 SM (d18:1/18:0)	58.02 ± 3.42	45.16 ± 3.41	47.42 ± 4.17	54.98 ± 20.28	61.32 ± 5.19
24:0 SM (d18:1/24:0)	79.01 ± 13.99	84.27 ± 9.33	85.53 ± 19.17	95.35 ± 8.17	99.82 ± 31.30
C16 Ceramide (d18:1/16:0)	49.28 ± 5.93	51.56 ± 8.26	53.52 ± 8.09	59.11 ± 11.52	51.73 ± 8.69
C18 Ceramide (d18:1/18:0)	5.35 ± 0.81	5.09 ± 0.86	5.34 ± 0.81	7.16 ± 0.73*	5.42 ± 1.03
C20 Ceramide (d18:1/20:0)	6.22 ± 0.81	6.36 ± 0.76	6.79 ± 1.03	9.58 ± 0.79*	6.60 ± 1.25
C22 Ceramide (d18:1/22:0)	8.31 ± 1.16	8.34 ± 0.67	8.64 ± 1.26	14.31 ± 4.02*	8.80 ± 1.39
C24 Ceramide (d18:1/24:0)	12.34 ± 1.59	13.53 ± 1.84	14.11 ± 1.81	30.30 ± 5.12*	16.82 ± 2.69
S1P	0.55 ± 0.12	0.34 ± 0.05	2.61 ± 0.40**	0.28 ± 0.14	1.18 ± 0.36#
C1P	0.38 ± 0.12	0.31 ± 0.03	0.64 ± 0.06**	0.12 ± 0.03*	0.45 ± 0.09##

All values mean ± SD, n=6 different measurements. Measured levels are ng/mg protein. Cells were treated with DMSO (1 μL/mL), SsnB (25 μM), and/or PMA (10 nM) for 12 h. SM, sphingomyelin; S1P, sphingosine-1-phosphate; C1P, ceramide-1- phosphate; Sparstolonin B (SsnB); Dimethyl Sulfoxide (DMSO); Phorbol 12-myristate 13-acetate (PMA). Statistical analysis was by One Way Analysis of Variance and all pairwise multiple comparison procedures were done by Tukey test. *, p<0,01 vs. Control, DMSO, PMA and PMA + SsnB. **, p<0,01 vs. Control, DMSO, SsnB and PMA + SsnB. #, p<0,01 vs. Control, DMSO, and SsnB. ##, p<0.05 vs. DMSO and SsnB.

 doi:10.20944/preprints202501.2224.v1

3. Discussion

The results of this study show that treating HCT-116 cells with 10 nM PMA for 12 h significantly increased cell proliferation. There was no significant change in cell proliferation in BJ fibroblast cells that received PMA at the same dose and time. PMA is a protein kinase C (PKC) activator and regulates cell proliferation and biological processes such as apoptosis by PKC activation [21–23]. Incubation of HCT-116 cells with 25 μM SsnB for 12 hours significantly reduced cell proliferation in the presence and absence of PMA. No statistically significant change in cell proliferation occurred in the presence and absence of PMA in BJ fibroblast cells treated with SsnB at the same dose and period. Studies have shown that the administration of SsnB to cancer and endothelial cells reduces cell proliferation [24–28] SsnB has been reported to inhibit cancer-related processes such as cell migration, invasion, and angiogenesis by stopping the cell cycle at G1 or G2/M checkpoints [26]. Administration of SsnB at concentrations between 10-100 μM has been found to show potent antiproliferative effects in various cell types, including neuroblastoma [4], prostate cancer [24,28] and pancreatic cancer [27] models. Within our literature review, this study is the first to examine PMA-dependent proliferation of SsnB in HCT-116 human colon cancer and healthy BJ fibroblast cells.

A significant increase in the intracellular levels of C18, C20, C22 and C24 ceramides occurred in HCT-116 cells treated for 12 h with a concentration of 25 μM of SsnB compared to all experimental groups. This is the first study to evaluate the impact of SsnB on endogenous sphingolipid levels in human colon cancer cells. Most of the research on SsnB concentrates on its anti-proliferative, anti-inflammatory, and anti-angiogenic properties, which are mainly achieved via inhibiting NF-κB and STAT1 signaling [29] and modifying Toll-like receptor (TLR) pathways [15]. When TLR4 or TLR1/TLR2 or TLR2/TLR6 ligands were used to stimulate mouse macrophages, SsnB significantly reduced the production of inflammatory cytokines [15]. Evaluated research has not provided sufficient evidence on the effects of SsnB on lipid metabolism or ceramide levels. Ceramide production in cancer cells and TLR signaling have a complicated interaction. According to certain studies, there may be a connection between TLR signaling and the metabolism of sphingolipids, particularly the synthesis of ceramide, which is involved in cancer treatment [30]. There aren't many solid examples of TLR antagonists directly boosting ceramide synthesis, though. Increased TLR expression has been linked to oncogenesis and the progression of cancer in cancer cell lines [31]. TLRs regulate the inflammatory responses in cancer cells. However, there is ongoing debate over the connection between TLR and cancer. TLRs have been demonstrated to both accelerate and appear to slow the progression of cancer [32–34].

Toll-like receptors have emerged as critical players in cancer biology, making them appeal to therapeutic targets due to their elevated expression in various tumors, including human colon cancer [8]. TLR2, TLR3, and TLR4 are overexpressed in most colon cancer cells [35]. However, in the context of colon cancer, aberrant TLR signaling has been linked to both tumor-promoting and tumor-suppressing effects, underscoring the complexity of targeting these pathways for therapeutic purposes [36]. For more than thirty years, bladder cancer has been treated with Bacillus Calmette-Guérin (BCG), the TLR2/TLR4 agonist that is the most effective TLR ligand in cancer therapy [37]. Its effectiveness highlights the therapeutic potential of TLR pathway modulation in oncology. During tumor development, TLR4 activation promotes the production of proinflammatory chemokines and immunosuppressive cytokines in an unregulated manner. This environment facilitates immune evasion, angiogenesis, and metastasis, as observed in human colon cancer [38]. These findings highlight the potential of TLR4 antagonists as a novel therapeutic strategy. Our findings suggest that manipulating TLR signaling holds significant therapeutic promise, particularly through the modulation of ceramide synthesis. Ceramide, a bioactive lipid, plays a crucial role in inducing cancer cell death and overcoming drug resistance [39]. In the context of TLR signaling, the small molecule SsnB has been hypothesized to influence ceramide synthesis, thereby enhancing ceramide-driven apoptosis in colon cancer cells. This mechanism involves TLR inhibition to create a pro-apoptotic environment characterized by ceramide accumulation, which, coupled with attenuated survival signaling, selectively induces apoptosis in cancer cells. Such dual modulation underscores the

 doi:10.20944/preprints202501.2224.v1

potential of SsnB as a targeted therapeutic agent in colon cancer characterized by dysregulated TLR pathways and survival mechanisms.

We discovered that administering 25 μM SsnB to colon cancer cells for 12 hours dramatically reduced their S1P and C1P levels. As far as we are aware, our study is the first to show that colon cancer cells treated with SsnB had lower S1P levels. Examples of functional sphingolipid metabolites that are vital to the biological pathways that are fundamental to the pathophysiology of cancer are C1P and S1P [40]. Both S1P and C1P sets off mechanisms that transform it into a lipid that promotes cancer [41].

We observed that MyD88, p-ERK, p-NF-kB, TNF-α, IL-1β, and IL-6 were significantly suppressed in cancer cells treated with SsnB compared to the control groups. These findings align with previous studies indicating that SsnB inhibits key inflammatory and survival pathways in cancer cells [18]. The MyD88/NF-kB signaling axis is a central pathway in regulating inflammatory responses and tumor progression in colorectal cancer [42]. Activation of MyD88, an adaptor protein, triggers a signaling cascade involving p-ERK and NF-kB, leading to the production of pro-inflammatory cytokines such as TNF-α, IL-1β, and IL-6 [43]. These cytokines not only promote a pro-tumorigenic microenvironment but also enhance cancer cell proliferation, survival, and metastasis [43]. The suppression of MyD88 and downstream mediators like p-ERK and p-NF-kB by SsnB suggests a potent anti-inflammatory effect, which could disrupt the tumor-supportive inflammatory milieu. Notably, NF-kB is often constitutively activated in various cancers, contributing to the expression of genes involved in cell survival, invasion, and chemoresistance [44]. By inhibiting NF-kB activation, SsnB may diminish the expression of its target cytokines, including TNF-α, IL-1β, and IL-6, which are critical for maintaining cancer cell viability and immune evasion.

Our results also highlight the therapeutic potential of SsnB in targeting cytokine-mediated pathways. TNF-α and IL-1β, key pro-inflammatory cytokines, are known to enhance angiogenesis, tumor invasion, and resistance to apoptosis. IL-6 further supports tumor growth through the activation of STAT3, a transcription factor implicated in cancer cell proliferation and metastasis in colorectal cancer cells [45]. The downregulation of these cytokines by SsnB may mitigate their tumor-promoting effects and enhance cancer cell susceptibility to apoptosis.

In summary, SsnB exerts its anti-cancer effects by downregulating MyD88, p-ERK, and p-NFκB signaling, along with suppressing the pro-inflammatory cytokines TNF-α, IL-1β, and IL-6. This comprehensive inhibition disrupts the tumor-supportive microenvironment and enhances apoptosis, offering a promising therapeutic approach for cancer treatment. This study's limitations include its reliance on HCT-116 cancer cells and BJ fibroblasts, which do not fully represent cancer heterogeneity or normal cell behavior. The in vitro model cannot replicate complex in vivo tumor dynamics, including immune and stromal interactions. PMA, used to induce inflammation, may not mimic natural tumor promotion. The limited dose range and treatment duration for SsnB leave long-term efficacy and safety unexplored.

4. Materials and Methods

4.1. Cell Culture

Human colon cancer (HCT-116) and healthy human fibroblast cell lines (BJ) were obtained from the American Type Culture Collection (ATCC; Manassas, VA, USA). Cells were cultured in 25 cm2 culture flasks using Dulbecco's Modified Eagle's Medium (DMEM, Sigma, Cat. #D5648, St. Louis, MO, USA) with high glucose. The medium was supplemented with, 3.7 g/L sodium bicarbonate (Sigma-Adrich), 10% (v/v) heat-inactivated fetal bovine serum (FBS) (Gibco, Life Technologies, Grand Island, NY, USA), 100 U/mL penicillin (Gibco), 100 μg/mL streptomycin (Gibco), 1% sodium pyruvate (Gibco) and 5 μg/100 mL amphotericin B (Gibco). The prepared medium was sterilized by vacuum filtering through a 0.22 μm bottle-top filter and stored at 4°C. The cells were incubated at 37°C with 5% CO_2 and 95% humidified air. When cells reach 80% density, they were lifted from the flask surface via trypsin-EDTA (0.05% Trypsin/0.02% EDTA; Gibco) and suspended and passed to new flasks.

 doi:10.20944/preprints202501.2224.v1

4.2. Application of Sparstolonin B and Phorbol 12-Myristate 13-Acetate

Five mg SsnB (MW= 268.22 g/mol; Merck Millipore, Cork, Ireland, #SML1767) was dissolved in 1.854 ml of DMSO to yield a stock concentration of 10 mM. The prepared main stock was diluted with DMSO to create an intermediate stock of 1 mM. One mM SsnB was diluted with cell culture medium to concentrations of 3.125, 6.25, 12.5, 25 and 50 µM. MTT [3-(4,5-dimethylthiazol-2-yl)-2,5-diphenyltetrazolium bromide] cell viability analysis was used to determine the dose and duration of application.

Five mg PMA (MW= 616.83 g/mol; LC Laboratories, Canada, #P-1680) was dissolved in 1 ml DMSO to prepare a stock concentration of 8.1 mM. The prepared main stock was diluted with DMSO to create an intermediate stock of 1 mM. One mM of PMA intermediate stock was diluted with cell culture medium to concentrations of 1, 5, and 10 nM. Dose and duration of administration were determined by MTT analysis.

4.3. Cell Viability Analysis

MTT (Gold Biotechnology Inc., St. Louis, MO, USA) was dissolved at a concentration of 5 mg/mL in PBS and sterilized by passing through a filter with a pore diameter of 0.22 µm. Before MTT analysis, HCT-116 and BJ fibroblast were plated in 96 well plates and waited for one night to adhere. After adhesion, 200 µl of cell culture medium containing either DMSO (1 µL/mL), PMA (1-10 nM) and/or SsnB (3.125-50 µM) were added to the wells. After 12-18 hours of incubation, the media were withdrawn, fresh medium containing MTT was added (90 µL medium + 10 µL MTT with a total volume of 100 µL) and the 96 well plate was incubated for 2 hours. Purple formazan crystals formed at the bottom of the wells were dissolved with 100 µL of DMSO and absorbance was measured at 570 and 690 nm via a spectrophotometric plate reader (MicroQuant, Bio-Tek Instruments Inc., Charlotte, VT, USA). The percentage of cell viability was calculated so that the absorbance in the control group represented 100% cell viability [Cell viability (%) = (Abs sample / Abs control) x 100]. According to the results of the MTT test, five different experimental groups were formed for each cell line.

4.4. Immunofluorescence Staining

Approximately 100,000 cells/well were plated in an 8 well chamber slide (Merck Millipore, Cork, Ireland) and cells were allowed to adhere overnight. Following 12 hour incubation of treatment groups, cells were washed 2 times with cold PBS and were fixed in 4% paraformaldehyde (Sigma-Aldrich, St. Louis, MO, USA) solution for 10 minutes. After two washes in PBS, cells were permeabilized in 0.2% Triton-X-100 (Sigma-Aldrich, St. Louis, MO, USA) for 10 min and washed five times with PBS. Afterwards, 5% normal goat serum (NGS; Vector Laboratories, Burlingame, CA, USA) was used for blocking for 30 minutes, 200 µl of primary antibody was applied, and the chamber slide was kept at 4°C overnight. Primary antibodies were diluted with ab-diluent (PBS containing 5% NGS and 0.2% Tween 20). The primary antibodies used were PCNA rabbit polyclonal ab (1:100 dilution, #bs-0754R, Bioss Antibodies Inc., Woburn, MA, USA), phospho-ERK1/2 (Thr202/Tyr204) rabbit polyclonal ab (1:200 dilution, #AF1015, Affinity Biosciences, Changzhou, Jiangsu, China), phospho-NF-kB rabbit polyclonal ab (1:200 dilution, #AF2006, Affinity Biosciences, Changzhou, Jiangsu, China), MyD88 rabbit polyclonal ab (1:100 dilution, # BT-AP05682, BT Lab, Shanghai, China) and cleaved-caspase 3 rabbit polyclonal ab (1:100 dilution, #9664S, Cell Signaling Tech., Massachusetts, USA). After the primary antibody incubation, the incubation medium was withdrawn, 3 washes were performed with PBS, and 200 µl of fluorophore-labeled secondary antibody (Alexa Fluor, 1:1000 dilution, ab150077 Abcam, Cambridge, UK) was added. Cells were incubated at room temperature for 45 minutes and after incubation, cells were washed with PBS 2 times and a drop of DAPI was applied (Fluoroshield with DAPI #F6057, Sigma Aldrich, St. Louis, MO, USA) to stain cell nuclei. The slides were covered with coverslips without air bubbles. Imaging was performed with a fluorescence microscope (Olympus BX61 fully automated, Tokyo, Japan) using DP controller software. Alexa Fluor was imaged at 488 nm excitation and 505-525 nm emission, while

 doi:10.20944/preprints202501.2224.v1

DAPI was imaged at 350 nm excitation and 440-460 nm emission. Fluorescence was measured using NIH ImageJ 1.53e software and calculated with the formula CTCF (corrected total cell fluorescence) = ID (integrated density)- [ASC (area of selected cell) x BMF (background mean fluorescence)].

4.5. Determination of TLR 2 and TLR 4 mRNA Expression

OMIM (Online Mendelian Inheritance in Man) database was used as a source for all mRNA sequences. OligoYap 9.0 software (SNP Biotechnology R&D Ltd., Ankara, Turkey) was used to design primers and probes. Supplementary Table S1 lists the primers and probes that were used. The One-run RT PCR kit (SNP Biotechnology R&D Ltd., Ankara, Turkey) was used to conduct real-time PCR analysis. Several forward and reverse primer concentrations were used in the optimization process to determine the lowest primer concentration that would produce the highest ΔRn (the difference between the sample's minimum and maximum fluorescence). Using various probe concentrations at the ideal primer concentrations allowed for the determination of the ideal probe concentration. The concentration of the probe that yielded the lowest cycle threshold (Ct) value was found to be the optimal one.

Total RNA extraction was performed using a commercial kit and the manufacturer's instructions (SNP Biotechnology R&D Ltd., Ankara, Turkey). The extracted RNA was dissolved in 70 µL of TE buffer [10 mM Tris-HCl, 0.1 mM EDTA (pH 7.5)]. 10 µL of the dissolved RNA was diluted with 490 µL of distilled water (1:50 dilution). The diluted RNA sample was tested for absorbance at 260 and 280 nm using spectrophotometry. The purity of the RNA samples was assessed using the test results at 260 and 280 nm. Samples with a 260 nm/280 nm ratio of less than two were suitable for analysis. The absorbance at 260 nm was used to calculate the samples' RNA content. At 260 nm, 40 µg/mL of RNA was equivalent to an absorbance unit of 1. Sample RNA (100 ng/µL), one-run mix, primer-1 (100 pmol), primer-2 (100 pmol), and probe (100 pmol) were all included in the sample preparation for each assay.

RT-PCR analysis was performed using the Mx3000p Multiplex Quantitative PCR system (Stratagene, CA, USA). The cycle conditions were as follows: step 1, 10 minutes at 42 °C (1 cycle); step 2, 5 seconds at 90 °C and step 3, 45 seconds at 60 °C (40 cycles). Using MxPro QPCR Software for the Mx3000P system, the log-linear phase of amplification was monitored to obtain Ct values for each RNA sample. All reactions were conducted in three repetitions, and the mRNA levels of each gene normalized to beta actin were expressed as a $2^{-(\Delta\Delta ct)}$ fold change.

4.6. ELISA Measurements

PCNA was determined with a non-competitive sandwich ELISA kit (cat. #ELK5141 Biotechnology; Denver, CO, USA). HCT-116 and BJ fibroblasts (10^7 cell/mL) were subjected to ultrasonication, and supernatants were collected by centrifugation at 4°C for 10 min at 1500 × g. The amount of PCNA was determined in accordance with the kit instructions and the samples were measured in a spectrophotometric plate reader at 450 nm. PCNA concentration in the samples was calculated using a standard curve and reported as ng/cell count.

Protein levels of TLR2 (cat # E0358Hu. BT Lab, Shanghai, China), TLR4 (cat # E0346Hu. BT Lab, Shanghai, China), MyD88 (cat. #E1870Hu BT Lab, Shanghai, China), TNF-α (cat. #E0082Hu. BT Lab, Shanghai, China), IL-1β (cat # E0143Hu BT Lab, Shanghai, China) and IL-6 (cat. #E0090Hu BT Lab, Shanghai, China) were assessed using sandwich ELISA kits in cell lysates. Cell pellets from the experimental groups were suspended in 250 µL of cold PBS for the cell samples. Sonication (Bandelin Sonopuls HD 2070, Bandelin Elec., Germany) broke up the cells totally. After centrifuging the lysates at 1500 × g for 10 minutes at 2–8°C, the supernatants were gathered. Spectrophotometric absorbance measurements were made at 450 nm using the measurement procedures outlined in the kit manuals. To analyze sample concentrations on nonlinear standard curves, GraphPad Prism software was used for curve fitting and interpolation. The results were expressed in milligrams of cell protein.

 doi:10.20944/preprints202501.2224.v1

4.7. TUNEL Analysis

Cell death was detected using the One-Step TUNEL Assay Kit (Elabscience; Houston, Texas, USA, E-CK-A320). This technique relies on the use of fluorescent markers to identify double-stranded DNA breaks that take place in apoptotic cells. The test protocol was followed in the preparation of each sample and reagent. On chamber slides (Merck Millipore, Cork, Ireland), 100,000 cells were transferred per well. After treatment and incubation according to experimental groups, the cells were fixed using fixative buffer (paraformaldehyde) for 20 minutes at room temperature. The slides were washed three times with PBS for five minutes each after fixation. DNase I (200 U/mL) was added to create positive controls, which were then incubated for 25 minutes at 37°C. Negative controls did not receive TdT Enzyme treatment; instead, they were incubated with an identical volume of buffer. All other groups received 100 µL of TdT, which was then incubated for 25 minutes at 37°C. Following incubation, each slide received 50 µL of labeling working solution, which was then incubated for 60 minutes at 37°C in a humidified environment. The slides then went through three 5-minute PBS washes. Upon the removal of the chambers and a tissue-cleaning procedure, a drop of DAPI (Sigma-Aldrich; St. Louis, MO, USA) was applied to each slide. A fluorescence microscope (Olympus BX61 fully automated, Tokyo, Japan) was used to view the fluorescence intensity after a clean, air-bubble-free coverslip was put in place.

4.8. Determination of Apoptotic Cells by Flow Cytometry

The apoptotic effects of PMA and SsnB on HCT-116 and BJ cells were assessed using an Annexin-V/PI apoptosis kit (Elabscience: #E-CK-A211, Texas, USA). Cells were treated as previously described, washed with PBS, and detached using Trypsin-EDTA. After suspension in PBS, 1×10^6 cells were transferred to flow cytometry tubes, washed twice, and centrifuged at 125×g for 5 minutes. The supernatant was discarded, and cells were resuspended in 500 µL Annexin-V binding buffer. Annexin-V-FITC (5 µL) and PI (5 µL) were added, and the mixture was incubated for 20 minutes at room temperature. Fluorescently labeled cells were analyzed immediately on the FACS Canto II flow cytometer (BD Biosciences, San Jose, CA, USA) with appropriate settings. Data were processed using BD FACS Diva 6.1.3 software, and results were expressed as percentages of total cell staining.

4.9. Sphingolipidomic Analysis

Samples were prepared for SM and CER analysis as previously described [46]. Cell lysates (100 mg/ml protein) were mixed with 2 µL of a 5000 ng/mL internal stock solution, and then 375 µL of chloroform:methanol (1:2, v/v) was added. After 30 seconds of sonication and 5 minutes of vortexing with 100 µL of distilled water, the mixture was allowed to rest at room temperature for 30 minutes. The mixture was centrifuged at 2000 × g for five minutes after incubation, and the supernatant was gathered. After adding 125 µL of distilled water and 125 µL of chloroform, the supernatant was vortexed and allowed to sit at room temperature for an additional half hour. After incubation, a nitrogen stream (VLM, Bielefeld, Germany) was used to dry 500 µL of the top organic layer in a new glass tube. The dried residue was dissolved in 100 µL of methanol:formic acid (99.9:0.1) and then placed into insert vials for LC-MS/MS analysis.

Ceramide and sphingomyelin levels were measured using an LC/MSMS instrument (LCMS-8040, Shimadzu Corporation, Japan) paired with an ultra-fast liquid chromatography system (LC-20 AD UFLC XR) [46]. Standards were obtained from Avanti Polar Lipids, with a labeled internal standard (C16 CER d18:1/16:0) from Cambridge Isotope Laboratories. Sphingolipid standards were prepared by sonication at 40°C in methanol. Chromatographic separation was achieved on an XTerra C18 HPLC column (2.1 mm × 50 mm, Waters, MA, USA) at 60°C with a 10 µL injection volume and a 0.450 mL/min flow rate. Gradient elution lasted 30 minutes with mobile phases of water/acetonitrile/2-propanol and acetonitrile/2-propanol. Positive electrospray ionization (ESI) and multiple reaction monitoring (MRM) were used for detection. Calibration ranges were linear between 39–625 ng/mL.

 doi:10.20944/preprints202501.2224.v1

4.10. Protein Measurements

The protein concentration in all samples were determined at 595 nm via Coomassie reagent (Thermo Scientific; Rockford, USA). Bovine Serum Albumin was used as standard in this measurement.

4.11. Statistical Analyses

SigmaPlot 15 or GraphPad Prism 8.4.3 were used for statistical analyses. Normality tests determined data distribution. Non-parametric tests were used for non-normal data. Experimental groups were compared using Kruskal-Wallis or One-Way ANOVA, followed by post-hoc tests to identify specific group differences when significant differences were found. Results are detailed in figure legends.

Supplementary Materials: The following supporting information can be downloaded at the website of this paper posted on Preprints.org.

Author Contributions: B.Ç.: methodology, validation, formal analysis and investigation. Ç.Y.: methodology, software, formal analysis and investigation. T.Ç.: methodology, software, formal analysis and investigation. Z.B.: conceptualization, supervision and review. E.K.: conceptualization, supervision and review. M.A.: conceptualization, funding acquisition, supervision, writing, reviewing and editing.

Funding: This research was funded by Akdeniz University Scientific Research Projects Coordination Unit (BAP) grant number: TDK-2024-6590, Health Institutes of Turkey (TÜSEB)) grant number: 31481 and The Scientific and Technological Research Council of Turkey (TUBITAK)) grant number: 124S394.

Institutional Review Board Statement: Not applicable.

Informed Consent Statement: Not applicable.

Data Availability Statement: Data obtained and analyzed in this work are available from the corresponding author upon reasonable request.

Conflicts of Interest: The authors declare no conflicts of interest.

Abbreviations

C1P, ceramide-1-phosphate; Ct, cycle threshold; ELISA, enzyme-linked immunosorbent assay; ESI, electrospray ionization; IL-1β, interleukin-1 beta; IL-6, interleukin-6; MRM, multiple reaction monitoring. PAMPs, pathogen-associated molecular patterns; PCNA, proliferating cell nuclear antigen; p-ERK, phosphorylated extracellular signal-regulated kinase; PMA, phorbol 12-myristate 13-acetate; p-NF-kB, phosphorylated nuclear factor kappa-light-chain-enhancer of activated B cells; S1P, sphingosine-1-phosphate; SsnB, Sparstolonin B; TLR, toll-like receptor; TNF-α, tumor necrosis factor-alpha and cytokines; WHO, World Health Organization.

References

1. Sung H, Ferlay J, Siegel RL, Laversanne M, Soerjomataram I, Jemal A, Bray F. Global Cancer Statistics 2020: GLOBOCAN Estimates of Incidence and Mortality Worldwide for 36 Cancers in 185 Countries. CA Cancer J Clin. 2021 May;71(3):209-249. doi: 10.3322/caac.21660. Epub 2021 Feb 4. PMID: 33538338.
2. Mileo AM, Nisticò P, Miccadei S. Polyphenols: Immunomodulatory and Therapeutic Implication in Colorectal Cancer. Front Immunol. 2019 Apr 11;10:729. doi: 10.3389/fimmu.2019.00729. PMID: 31031748; PMCID: PMC6470258.
3. Niedzwiecki A, Roomi MW, Kalinovsky T, Rath M. Anticancer Efficacy of Polyphenols and Their Combinations. Nutrients. 2016 Sep 9;8(9):552. doi: 10.3390/nu8090552. PMID: 27618095; PMCID: PMC5037537.
4. Kumar A, Fan D, Dipette DJ, Singh US. Sparstolonin B, a novel plant derived compound, arrests cell cycle and induces apoptosis in N-myc amplified and N-myc nonamplified neuroblastoma cells. PLoS One. 2014

May 1;9(5):e96343. doi: 10.1371/journal.pone.0096343. Erratum in: PLoS One. 2016 Jul 6;11(7):e0159082. doi: 10.1371/journal.pone.0159082. PMID: 24788776; PMCID: PMC4006872.
5. Yepuri N, Dhawan R, Cooney M, Pruekprasert N, Meng Q, Cooney RN. Sparstolonin B: A Unique Anti-Inflammatory Agent. Shock. 2019 Dec;52(6):568-576. doi: 10.1097/SHK.0000000000001326. PMID: 30807526.
6. PubChem. Available online: https://pubchem.ncbi.nlm.nih.gov (accessed on 28 January 2025).
7. Akira S, Takeda K, Kaisho T. Toll-like receptors: critical proteins linking innate and acquired immunity. Nat Immunol. 2001 Aug;2(8):675-80. doi: 10.1038/90609. PMID: 11477402.
8. Fukata M, Chen A, Vamadevan AS, Cohen J, Breglio K, Krishnareddy S, Hsu D, Xu R, Harpaz N, Dannenberg AJ, Subbaramaiah K, Cooper HS, Itzkowitz SH, Abreu MT. Toll-like receptor-4 promotes the development of colitis-associated colorectal tumors. Gastroenterology. 2007 Dec;133(6):1869-81. doi: 10.1053/j.gastro.2007.09.008. Epub 2007 Sep 14. PMID: 18054559; PMCID: PMC2180834.
9. Cammarota R, Bertolini V, Pennesi G, Bucci EO, Gottardi O, Garlanda C, Laghi L, Barberis MC, Sessa F, Noonan DM, Albini A. The tumor microenvironment of colorectal cancer: stromal TLR-4 expression as a potential prognostic marker. J Transl Med. 2010 Nov 8;8:112. doi: 10.1186/1479-5876-8-112. PMID: 21059221; PMCID: PMC2997091.
10. Doan HQ, Bowen KA, Jackson LA, Evers BM. Toll-like receptor 4 activation increases Akt phosphorylation in colon cancer cells. Anticancer Res. 2009 Jul;29(7):2473-8. PMID: 19596916; PMCID: PMC2901163.
11. Guo H, Chen Y, Hu X, Qian G, Ge S, Zhang J. The regulation of Toll-like receptor 2 by miR-143 suppresses the invasion and migration of a subset of human colorectal carcinoma cells. Mol Cancer. 2013 Jul 17;12:77. doi: 10.1186/1476-4598-12-77. PMID: 23866094; PMCID: PMC3750391.
12. Liu YD, Ji CB, Li SB, Yan F, Gu QS, Balic JJ, Yu L, Li JK. Toll-like receptor 2 stimulation promotes colorectal cancer cell growth via PI3K/Akt and NF-κB signaling pathways. Int Immunopharmacol. 2018 Jun;59:375-383. doi: 10.1016/j.intimp.2018.04.033. Epub 2018 Apr 24. PMID: 29689497.
13. Chung YH, Kim D. Enhanced TLR4 Expression on Colon Cancer Cells After Chemotherapy Promotes Cell Survival and Epithelial-Mesenchymal Transition Through Phosphorylation of GSK3β. Anticancer Res. 2016 Jul;36(7):3383-94. PMID: 27354597.
14. Guo Y, Zhou K, Zhuang X, Li J, Shen X. CDCA7-regulated inflammatory mechanism through TLR4/NF-κB signaling pathway in stomach adenocarcinoma. Biofactors. 2021 Sep;47(5):865-878. doi: 10.1002/biof.1773. Epub 2021 Aug 2. PMID: 34339079.
15. Liang Q, Wu Q, Jiang J, Duan J, Wang C, Smith MD, Lu H, Wang Q, Nagarkatti P, Fan D. Characterization of sparstolonin B, a Chinese herb-derived compound, as a selective Toll-like receptor antagonist with potent anti-inflammatory properties. J Biol Chem. 2011 Jul 29;286(30):26470-9. doi: 10.1074/jbc.M111.227934. Epub 2011 Jun 10. PMID: 21665946; PMCID: PMC3143611.
16. Wang M, Xiu L, Diao J, Wei L, Sun J. Sparstolonin B inhibits lipopolysaccharide-induced inflammation in 3T3-L1 adipocytes. Eur J Pharmacol. 2015 Dec 15;769:79-85. doi: 10.1016/j.ejphar.2015.10.050. Epub 2015 Oct 30. PMID: 26522926.
17. Piazzesi A, Afsar SY, van Echten-Deckert G. Sphingolipid metabolism in the development and progression of cancer: one cancer's help is another's hindrance. Mol Oncol. 2021 Dec;15(12):3256-3279. doi: 10.1002/1878-0261.13063. Epub 2021 Jul 29. PMID: 34289244; PMCID: PMC8637577.
18. Dilber Y, Çeker HT, Öztüzün A, Çırçırlı B, Kırımlıoğlu E, Barut Z, Aslan M. Sparstolonin B Reduces Estrogen-Dependent Proliferation in Cancer Cells: Possible Role of Ceramide and PI3K/AKT/mTOR Inhibition. Pharmaceuticals (Basel). 2024 Nov 21;17(12):1564. doi: 10.3390/ph17121564. PMID: 39770406; PMCID: PMC11677571.
19. Li F, Zhang N. Ceramide: Therapeutic Potential in Combination Therapy for Cancer Treatment. Curr Drug Metab. 2015;17(1):37-51. doi:10.2174/1389200216666151103120338. PMID: 26526831.
20. Ogretmen B. Sphingolipid metabolism in cancer signalling and therapy. Nat Rev Cancer. 2018 Jan;18(1):33-50. doi: 10.1038/nrc.2017.96. Epub 2017 Nov 17. PMID: 29147025; PMCID: PMC5818153.
21. Mosior M, Newton AC. Mechanism of interaction of protein kinase C with phorbol esters. Reversibility and nature of membrane association. J Biol Chem. 1995 Oct 27;270(43):25526-33. doi: 10.1074/jbc.270.43.25526. PMID: 7592722.
22. Tahara E, Kadara H, Lacroix L, Lotan D, Lotan R. Activation of protein kinase C by phorbol 12-myristate 13-acetate suppresses the growth of lung cancer cells through KLF6 induction. Cancer Biol Ther. 2009 May;8(9):801-7. doi: 10.4161/cbt.8.9.8186. Epub 2009 May 17. PMID: 19333010.
23. Hwang YP, Yun HJ, Choi JH, Kang KW, Jeong HG. Suppression of phorbol-12-myristate-13-acetate-induced tumor cell invasion by bergamottin via the inhibition of protein kinase Cdelta/p38 mitogen-activated protein kinase and JNK/nuclear factor-kappaB-dependent matrix metalloproteinase-9 expression. Mol Nutr Food Res. 2010 Jul;54(7):977-90. doi: 10.1002/mnfr.200900283. PMID: 19943262.

24. Liu S, Hu J, Shi C, Sun L, Yan W, Song Y. Sparstolonin B exerts beneficial effects on prostate cancer by acting on the reactive oxygen species-mediated PI3K/AKT pathway. J Cell Mol Med. 2021 Jun;25(12):5511-5524. doi: 10.1111/jcmm.16560. Epub 2021 May 5. PMID: 33951324; PMCID: PMC8184693.
25. Liu Q, Li J, Liang Q, Wang D, Luo Y, Yu F, Janicki JS, Fan D. Sparstolonin B suppresses rat vascular smooth muscle cell proliferation, migration, inflammatory response and lipid accumulation. Vascul Pharmacol. 2015 Apr-Jun;67-69:59-66. doi: 10.1016/j.vph.2015.03.015. Epub 2015 Apr 11. PMID: 25869499; PMCID: PMC4433853.
26. Bateman HR, Liang Q, Fan D, Rodriguez V, Lessner SM. Sparstolonin B inhibits pro-angiogenic functions and blocks cell cycle progression in endothelial cells. PLoS One. 2013 Aug 5;8(8):e70500. doi: 10.1371/journal.pone.0070500. PMID: 23940584; PMCID: PMC3734268.
27. Lyu Y, Duan B, Liu Z, Yang F, Chen C, Jiang X, Liu X. Sparstolonin B inhibits pancreatic adenocarcinoma through the NF-κB signaling pathway. Exp Cell Res. 2022 Aug 1;417(1):113214. doi: 10.1016/j.yexcr.2022.113214. Epub 2022 May 18. PMID: 35594953.
28. Takahashi I, Takagi K, Yamaguchi-Tanaka M, Sato A, Sato M, Miki Y, Ito A, Suzuki T. Toll-like receptor (TLR) 4 is a potent prognostic factor in prostate cancer associated with proliferation and invasion. Pathol Res Pract. 2024 Aug;260:155379. doi: 10.1016/j.prp.2024.155379. Epub 2024 May 29. PMID: 38850876.
29. Kim N, Kim C, Ryu SH, Kim GO, Bae JS. Anti-Inflammatory Effect of Sparstolonin B through Inhibiting Expression of NF-κB and STAT-1. Int J Mol Sci. 2022 Sep 6;23(18):10213. doi: 10.3390/ijms231810213. PMID: 36142124; PMCID: PMC9499357.
30. Schilling JD, Machkovech HM, He L, Sidhu R, Fujiwara H, Weber K, Ory DS, Schaffer JE. Palmitate and lipopolysaccharide trigger synergistic ceramide production in primary macrophages. J Biol Chem. 2013 Feb 1;288(5):2923-32. doi: 10.1074/jbc.M112.419978. Epub 2012 Dec 18. PMID: 23250746; PMCID: PMC3561515.
31. Sato Y, Goto Y, Narita N, Hoon DS. Cancer Cells Expressing Toll-like Receptors and the Tumor Microenvironment. Cancer Microenviron. 2009 Sep;2 Suppl 1(Suppl 1):205-14. doi: 10.1007/s12307-009-0022-y. Epub 2009 Aug 15. PMID: 19685283; PMCID: PMC2756339.
32. Onier N, Hilpert S, Arnould L, Saint-Giorgio V, Davies JG, Jeannin JF, Jeannin JF. Cure of colon cancer metastasis in rats with the new lipid A OM 174. Apoptosis of tumor cells and immunization of rats. Clin Exp Metastasis. 1999 Jun;17(4):299-306. doi: 10.1023/a:1006663017149. PMID: 10545016.
33. Garay RP, Viens P, Bauer J, Normier G, Bardou M, Jeannin JF, Chiavaroli C. Cancer relapse under chemotherapy: why TLR2/4 receptor agonists can help. Eur J Pharmacol. 2007 Jun 1;563(1-3):1-17. doi: 10.1016/j.ejphar.2007.02.018. Epub 2007 Feb 17. PMID: 17383632.
34. Zhang YB, He FL, Fang M, Hua TF, Hu BD, Zhang ZH, Cao Q, Liu RY. Increased expression of Toll-like receptors 4 and 9 in human lung cancer. Mol Biol Rep. 2009 Jul;36(6):1475-81. doi: 10.1007/s11033-008-9338-9. Epub 2008 Sep 2. PMID: 18763053.
35. Furrie E, Macfarlane S, Thomson G, Macfarlane GT; Microbiology & Gut Biology Group; Tayside Tissue & Tumour Bank. Toll-like receptors-2, -3 and -4 expression patterns on human colon and their regulation by mucosal-associated bacteria. Immunology. 2005 Aug;115(4):565-74. doi: 10.1111/j.1365-2567.2005.02200.x. PMID: 16011525; PMCID: PMC1782176.
36. Pradere JP, Dapito DH, Schwabe RF. The Yin and Yang of Toll-like receptors in cancer. Oncogene. 2014 Jul 3;33(27):3485-95. doi: 10.1038/onc.2013.302. Epub 2013 Aug 12. PMID: 23934186; PMCID: PMC4059777.
37. Yoo KH, Lim TJ, Chang SG. Monthly intravesical bacillus Calmette-Guérin maintenance therapy for non-muscle-invasive bladder cancer: 10-year experience in a single institute. Exp Ther Med. 2012 Feb;3(2):221-225. doi: 10.3892/etm.2011.400. Epub 2011 Dec 1. PMID: 22969872; PMCID: PMC3438621.
38. Li J, Yang F, Wei F, Ren X. The role of toll-like receptor 4 in tumor microenvironment. Oncotarget. 2017 Jul 8;8(39):66656-66667. doi: 10.18632/oncotarget.19105. PMID: 29029545; PMCID: PMC5630445.
39. Wajapeyee N, Beamon TC, Gupta R. Roles and therapeutic targeting of ceramide metabolism in cancer. Mol Metab. 2024 May;83:101936. doi: 10.1016/j.molmet.2024.101936. Epub 2024 Apr 9. PMID: 38599378; PMCID: PMC11031839.
40. Li RZ, Wang XR, Wang J, Xie C, Wang XX, Pan HD, Meng WY, Liang TL, Li JX, Yan PY, Wu QB, Liu L, Yao XJ, Leung EL. The key role of sphingolipid metabolism in cancer: New therapeutic targets, diagnostic and prognostic values, and anti-tumor immunotherapy resistance. Front Oncol. 2022 Jul 27;12:941643. doi: 10.3389/fonc.2022.941643. PMID: 35965565; PMCID: PMC9364366.
41. Pralhada Rao R, Vaidyanathan N, Rengasamy M, Mammen Oommen A, Somaiya N, Jagannath MR. Sphingolipid metabolic pathway: an overview of major roles played in human diseases. J Lipids. 2013;2013:178910. doi: 10.1155/2013/178910. Epub 2013 Aug 4. PMID: 23984075; PMCID: PMC3747619.
42. Wang L, Yu K, Zhang X, Yu S. Dual functional roles of the MyD88 signaling in colorectal cancer development. Biomed Pharmacother. 2018 Nov;107:177-184. doi: 10.1016/j.biopha.2018.07.139. Epub 2018 Aug 4. PMID: 30086464.

43. Tanimura A, Nakazato A, Tanaka N. MYD88 signals induce tumour-initiating cell generation through the NF-κB-HIF-1α activation cascade. Sci Rep. 2021 Feb 17;11(1):3991. doi: 10.1038/s41598-021-83603-4. PMID: 33597599; PMCID: PMC7890054.
44. Xia Y, Shen S, Verma IM. NF-κB, an active player in human cancers. Cancer Immunol Res. 2014 Sep;2(9):823-30. doi: 10.1158/2326-6066.CIR-14-0112. PMID: 25187272; PMCID: PMC4155602.
45. Chung SS, Wu Y, Okobi Q, Adekoya D, Atefi M, Clarke O, Dutta P, Vadgama JV. Proinflammatory Cytokines IL-6 and TNF-α Increased Telomerase Activity through NF-κB/STAT1/STAT3 Activation, and Withaferin A Inhibited the Signaling in Colorectal Cancer Cells. Mediators Inflamm. 2017;2017:5958429. doi: 10.1155/2017/5958429. Epub 2017 Jun 6. PMID: 28676732; PMCID: PMC5476880.
46. Aslan M, Polyunsaturated Fatty Acid and Sphingolipid Measurements by Tandem Mass Spectrometry, Mini-Reviews in Organic Chemistry; Mini-Reviews in Organic Chemistry, 18(1), 3-10. DOI: 10.2174/1570193X17999200504094901.